Solution Processing Cu_3BiS_3 Absorber Layers with a Thiol-Amine Solvent Mixture

Kristopher M. Koskela, Abegail C. Tadle,‡ Keying Chen,‡ and Richard L. Brutchey*

Department of Chemistry, University of Southern California, Los Angeles, CA 90089, United States

* Email: brutchey@usc.edu

‡ Authors contributed equally.

Keywords: solar absorber, Cu_3BiS_3, wittichenite, thin film, solution processing

ABSTRACT: There is a need to develop more Earth abundant, less toxic, and more environmentally stable solar absorbers as the market demand for solar cells increases. Wittichenite (Cu_3BiS_3) is a sulfosalt mineral that belongs to the Cu_3MCh_3 (*M* = Sb, Bi; *Ch* = S, Se) family of materials. Cu_3BiS_3 contains bismuth, a non-toxic heavy metal that has a $6s^2$ electronic structure akin to halide perovskites that have demonstrated excellent properties, and the sulfosalt crystallizes in the $P2_12_12_1$ space group with a near-optimal band gap for single junction thin film solar cells. We report the utility of thiol-amine solvent mixtures to dissolve inexpensive bulk CuO and Bi_2S_3 precursors to produce a free-flowing semiconductor ink. Good quality and phase pure Cu_3BiS_3 thin films were solution processed from this ink upon mild annealing. The *p*-type thin films possess a direct band gap of 1.47 eV with a high absorption coefficient through the visible (~10^5 cm^{-1}), carrier mobilities in the range of 0.4-90 cm^2 $(V•s)^{-1}$, and a strong photoelectrochemical current response. The optoelectronic properties of Cu_3BiS_3 thin films deposited using this thiol-amine chemistry suggest it is a favorable candidate as a solution processable solar absorber.

1. INTRODUCTION

With the increasing demand for solar energy conversion, there is a need for more Earth abundant, less toxic, and more environmentally stable solar absorbers.[1] State-of-the-art photovoltaics, like CdTe and $Cu(In,Ga)(S,Se)_2$ (CIGS), have appreciable power conversion efficiencies >20%, but are made up of toxic (i.e., Cd) or low Earth abundance elements (i.e., In, Ga, Te).[2,3] Recently, hybrid lead halide perovskite solar cells have demonstrated remarkable power conversion efficiencies > 22%, but, aside from containing lead, they possess significant challenges due to their intrinsic environmental instabilities to air and moisture.[4] Halide perovskite materials belong to a broader class of solar absorbers containing high-*Z* ns^2 cations.[4] Materials containing ns^2 cations have been theorized and demonstrated to have large band dispersions (good hybridization) that lead to high carrier mobility,[5] defect tolerance,[6] and enhanced dielectric constants[6] leading to improved carrier transport.

Chalcogenide solar absorbers containing ns^2 lone pairs (e.g., those with Sn^{2+}, Sb^{3+}, Bi^{3+} cations) hold promise as photovoltaic materials, including SnS,[7] $CuSbS_2$,[8] and Sb_2S_3.[9] Looking to other compositional variants of ns^2-containing chalcogenide solar absorbers, there is promise within the Cu-Bi-S phase space, such as $CuBiS_2$ and Cu_3BiS_3.[10] The Cu_3MCh_3 system (where, *M* = Sb, Bi and *Ch* = S, Se) is a potentially interesting material family for photovoltaic applications.[11] Wittichenite, the known sulfosalt mineral phase (Strunz 2.GA.20) of Cu_3BiS_3, is thermodynamically stable due to its natural occurrence and crystallizes in the orthorhombic $P2_12_12_1$ space group.[12] The crystal structure is composed of trigonal pyramidal BiS_3 units that have $6s^2$ lone pairs at the cap and are corner sharing with trigonal planar CuS_3 units forming continuous chains parallel to [001] and sheets normal to the [010] plane (**Figure 1**).[12] Density functional theory (DFT) calculations suggest Cu_3BiS_3 has a higher absorption coefficient than either CIGS or Cu_2ZnSnS_4 (CZTS).[13] DFT also suggests that the valence band maximum (VBM) consists mostly of Cu *d* and S *p* states with little impact from Bi *s* states, while the conduction band minimum (CBM) consists of mostly Bi *p* and S *p* antibonding states.[11] Wittichenite contains bismuth, which is a green heavy element due to its low toxicity/environmental impact and relative Earth abundance, where Bi reserves total 370,000 tons whereas In reserves total 15,000 tons (>300,000 tons when considering Zn co-deposits or lower

quality ores that are more difficult and expensive to extract).[14-17]

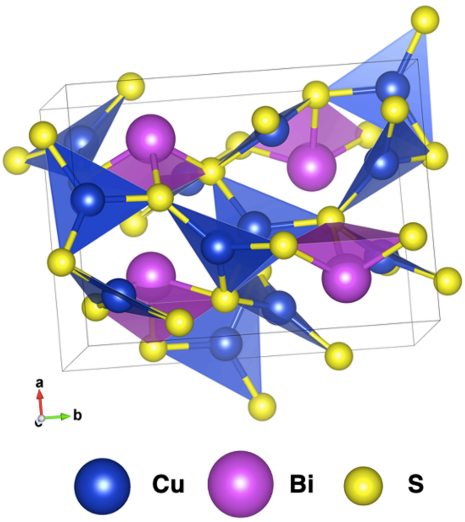

Figure 1. Crystal structure of wittichenite Cu_3BiS_3 (space group $P2_12_12_1$), from PDF exp. 43-1479.

Thin films of wittichenite Cu_3BiS_3 have been deposited by physical vapor deposition methods, including sputtering[18,19] and thermal evaporation,[11,20] but these methods are generally much more energy intensive and costly than solution processing.[21] While Cu_3BiS_3 thin films have been solution deposited with non-vacuum based techniques, such as spray pyrolysis,[22,23] electrodeposition,[24,25] and chemical bath deposition,[26,27] the solution deposition of Cu_3BiS_3 thin films is still challenged by the need for pre-synthesized, non-commercially available precursors,[23] extra post-deposition sulfurization steps,[24-27] amorphous films,[28] low absorption coefficients ($<10^5$ cm^{-1}),[29] and/or films with high band gaps (>1.6 eV).[22,30] To overcome some of the general issues with solution processing of chalcogenides, our group reported a binary solvent mixture (termed an "alkahest") comprised of thiols and amines that dissolves in excess of 100 different bulk materials, including metals, metal oxides, and metal chalcogenides, to form solution processable semiconductor inks.[31-37] A simple dissolve and recover approach can be used to produce chalcogenide thin films through solution deposition and mild annealing. In the absence of an external chalcogen source, the thiol acts as a competent sulfur source to produce polycrystalline metal sulfides. This thiol-amine method has been utilized for the solution deposition of both CIGS and CZTS solar cells with competitive power conversion efficiencies.[38-40] Here, we report the utility of thiol-amine solvent mixtures to dissolve CuO and Bi_2S_3 precursors to form an ink, which was solution processed to give phase-pure Cu_3BiS_3 thin films under mild annealing conditions. The thin films were assessed as solar absorber layers with a combination of optical, electronic, and photoelectrochemical measurements.

2. EXPERIMENTAL

2.1 Reagents.

Bismuth(III) sulfide (Bi_2S_3, 99.995%), copper(II) oxide (CuO, 99.99%), and 1,2-ethylenediamine (en, 99.5%) were bought from Sigma Aldrich. 1,2-Ethanedithiol (EDT, 98+%) was bought from Alfa Aesar. ICP standards for Cu and Bi (1000 ppm, 2% HNO_3) were bought from Perkin Elmer. Europium(III) nitrate pentahydrate (99.8%) was bought from Strem. All reagents were used as received.

2.2 Bulk Precursor Dissolution.

To generate the semiconductor ink, 18.1 mg (0.228 mmol) CuO and 19.4 mg (0.038 mmol) Bi_2S_3 were dissolved in 0.1 mL EDT and 0.4 mL en with stirring at 30 ˚C for 10 h under air (1 atm). If the solvents solidified upon addition to the bulk solid precursors, gentle heating can be used to re-liquify the ink.

2.3 Solution Processing.

Thin films were solution processed by spin coating onto ca. 1 cm^2 borosilicate glass, fluorine doped tin oxide (FTO), or silicon substrates that were pre-cleaned by bath sonication in acetone, isopropanol, and then ethanol (each for 10 min). The final ink (75 mg mL^{-1}) was spin coated onto the substrate at 2500 rpm for 1 min under N_2. The films were heated to 400 ˚C under N_2 in between coats, and allowed to return to room temperature before the next layer was deposited.

2.4 Property measurements.

Conductivity measurements were performed on Cu_3BiS_3 thin films (490 nm average thickness) deposited on a 1 cm^2 borosilicate substrates. Cu leads were attached to the four corners of the square thin film with colloidal Ag paste (Ted Pella, Inc.). A Quantum Design Physical Properties Measurement System (PPMS) regulated the thin film temperature and applied a magnetic field of 10000 Oe. A Keithley 2182A nanovoltmeter and a Keithley 6220 current source, controlled by a Keithley 7065 Hall effect card, were used to collect the conductivity data. Photoelectrochemical measurements were performed with FTO slides (Sigma Aldrich) with a conductivity of *ca.* 7 Ω sq^{-1} that were cut into 0.5×2.5 cm^2 pieces and were cleaned as described above. Kapton tape was used to mask off a portion of the substrate for electrode contact. Films of Cu_3BiS_3 were prepared as described above. Silver paint was used to attach a silver wire to the unmasked FTO substrate. Loctite epoxy was applied over the wire and around the edges of the film to mask these areas from solution and the electrodes were allowed to dry for 24 h before use. Photocurrent response measurements of the Cu_3BiS_3 thin films were collected with a VersaSTAT 3 potentiostat. The two-chambered glass photoelectrochemical cell contained a graphite rod counter electrode (Graphite Machining, Inc., Grade NAC-500 purified, < 10 ppm ash level), a Ag|AgCl (3 M KCl) reference electrode, and a Cu_3BiS_3 thin film on FTO-coated glass as the working electrode. The working and reference electrodes were placed in one chamber, which is separated from the counter electrode chamber by a fine porosity glass frit. The electrolyte consisted of aqueous 0.1 M $Eu(NO_3)_3$ as the sacrificial oxidant. The solution was sparged with N_2

via bubbling for 10 min before the experiments, and then N_2 was continuously flowed over the head space during the experiments. Simulated sunlight from an AM1.5G filtered 300 W xenon arc lamp (Asahi Spectra HAL-320W) was used to illuminate the sample from dark conditions.

3. RESULTS AND DISCUSSION

3.1 Semiconductor ink preparation and conversion.

To formulate the Cu_3BiS_3 semiconductor ink, as-purchased bulk powders of CuO and Bi_2S_3 were mixed in a 6:1 (mol/mol) ratio, respectively, and then dissolved in a mixture of ethanedithiol (EDT) and ethylenediamine (en) (1:4 vol/vol, respectively), with an overall solute concentration of 75 mg mL^{-1}. Different combinations of oxides and sulfides (e.g., Cu_2O, Cu_2S, Bi_2O_3) may also return phase pure Cu_3BiS_3, but CuO and Bi_2S_3 were chosen as bulk precursors due to these precursors yielding qualitatively better-quality thin films. The bulk powders of CuO and Bi_2S_3 both have approximate solubility limits in solvent combination of 10-15 wt% at 25 °C (1 atm). The semiconductor ink was stirred at 30 °C for 10 h to yield an optically clear, free flowing, burnt orange solution that does not scatter light (**Figure 2a**). The resulting ink was stable and precipitate-free when kept under ambient conditions for several days.

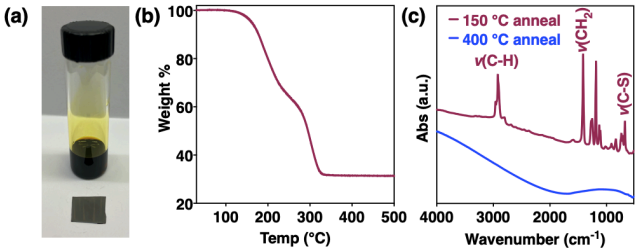

Figure 2. (a) Semiconductor ink containing bulk CuO and Bi_2S_3 dissolved in a 1:4 (vol/vol) mixture of EDT and en next to a Cu_3BiS_3 thin film. (b) Thermogravimetric analysis trace of the dried ink demonstrating a decomposition endpoint of < 350 ˚C. (c) FT-IR spectra of the ink dried at 150 ˚C and a thin film heated to 400 ˚C confirming loss of organic species.

Thermogravimetric analysis (TGA) was used to determine an endpoint of volatilization and decomposition for the solution deposited and dried ink. The dried ink begins mass loss at *ca.* 150 °C and it was found that mass loss terminated < 350 °C (**Figure 2b**). The loss of the organic species upon annealing the dried ink from 150 to 400 °C was corroborated using FT-IR spectroscopy (**Figure 2c**). IR bands were not observed in the dried ink above 3000 cm^{-1}, where ν(N–H) stretches are expected, suggesting that en, or protonated ammonium species, may be mostly absent after heating the ink to 150 ˚C. The strong IR bands of EDT present in the dried ink (*i.e.*, at 2930 cm^{-1} ν(C–H), 1420 cm^{-1} δ(CH_2), and 675 cm^{-1} ν(C–S)) are completely absent from the film after annealing to 400 °C.[35,37]

3.2 Cu_3BiS_3 thin films.

To demonstrate the effectiveness of EDT-en to solution process high-quality Cu_3BiS_3 thin films, the ink was used to sequentially deposit three identical coats by spin coating with a 400 °C anneal between each coat. The solution deposition procedure returned dark gray, specularly reflective polycrystalline thin films of Cu_3BiS_3 that are free of pinholes, microcracks, and other imperfections (e.g., edge effects or striations). A cross-sectional scanning electron microscopy image of a Cu_3BiS_3 thin film formed by depositing three coats of the semiconductor ink on Si/SiO_2 returns a 490 nm mean film thickness (**Figure S1**).

The dark gray material resulting from annealing to 400 °C was phase pure orthorhombic Cu_3BiS_3, as confirmed by powder X-ray diffraction (**Figure 3**). Rietveld refinement of the resulting diffraction pattern using the orthorhombic $P2_12_12_1$ space group returns lattice constants of a = 7.70410(8), b = 10.41840(10), and c = 6.71624(7) Å, with a unit cell volume of V = 539.075(6) $Å^3$ (**Table S1**). The refinement was not improved with the addition of any additional ternary phases (i.e., $CuBiS_2$) or binary phases of copper or bismuth sulfides, and the lattice constants for Cu_3BiS_3 agree with the values for bulk wittichenite (i.e., a = 7.723(10), b = 10.395(10), and c = 6.716(5) Å; V = 539.16 $Å^3$).[12] Raman spectroscopy corroborated the single phase nature of the resulting Cu_3BiS_3 thin film (**Figure S2**). Four Raman active modes were observed at 150, 248, 278, and 468 cm^{-1}, which match well with spectra previously reported for wittichenite.[11,41-43] Importantly, no Raman active bands were observed for any potential binary impurities of CuS,[44] $Cu_{2-x}S$,[45] or Bi_2S_3,[46] or potential ternary phases such as $CuBiS_2$.[47] ICP-OES was used to assess the elemental composition of the solution processed films. By averaging four separate analyses, the elemental stoichiometry of the resulting thin films was $Cu_{2.84}B_{1.00}S_3$; this is in the range of copper deficiencies that have been previously published for Cu_3BiS_3.[24,48]

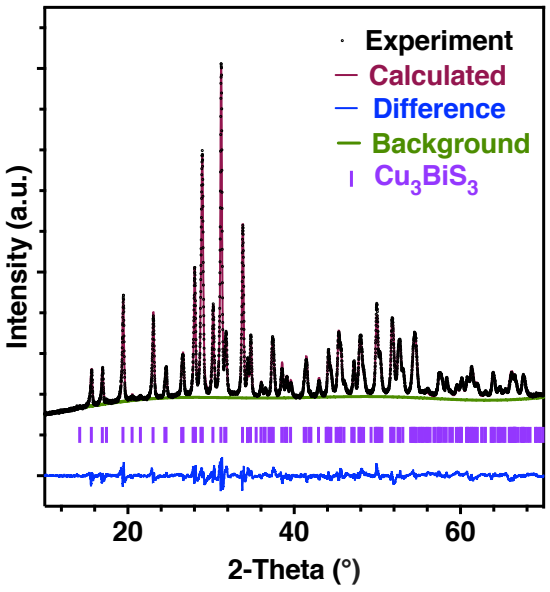

Figure 3. Rietveld refinement to the orthorhombic $P2_12_12_1$ structure of the powder X-ray diffraction pattern of phase pure Cu_3BiS_3. Open circles are experimental data, purple tick marks are individual reflections of the wittichenite structure, and the difference pattern is given in blue. (R_{WP} = 4.30%; G.O.F. = 2.14)

X-ray photoelectron spectroscopy (XPS) was employed to interrogate the valence states in our Cu_3BiS_3 thin films. A fitting procedure was used to accurately analyze the peaks, as most Cu_3BiS_3 thin films reported in the literature lack robust fitting of the peaks, possibly due to the Bi 4*f* and S 2*p* peak overlap or poor signal to noise.[25,43,49] An XPS survey scan of the Cu_3BiS_3 thin film that was exposed to air is given in the Supporting Information (**Figure S3**). High-resolution Cu 2*p*, Bi 4*f* and S 2*p*, and S 2*s* spectra and their corresponding peak fittings are given in **Figures S4-6**, respectively. In addition, the peak positions and spin orbit coupling splitting values are tabulated in **Table S2**. It is observed that the Cu 2*p* spectral region is best fit with a single set of doublets at 952.0 and 932.2 eV (peak splitting 19.8 eV), which corresponds to a single Cu^+ environment in our Cu_3BiS_3 thin film, and is consistent with a single Cu^+ environment in previously reported Cu_3BiS_3 thin films deposited by thermal evaporation and surface cleaned by Ar^+ ion sputtering for several hours under vacuum.[11,50] Surface oxidation of copper would return characteristic peaks at higher binding energy,[51] and as none are seen, we can confirm that no significant degree of surface copper oxidation has occurred under the film processing conditions.

The Bi 4*f* and S 2*p* spectra were fit using three sets of doublets. Two doublets correspond to two different Bi species, both with a splitting of 5.3 eV. The larger doublet at 163.4 and 158.1 eV corresponds to Bi^{3+} in a sulfide environment,[52] and is consistent with other Cu_3BiS_3 samples.[11,25] The smaller doublet at 163.9 and 158.6 eV corresponds to possible surface oxidized Bi species that may be an additional amorphous and/or non-stoichiometric oxide species on the surface due to Bi_2O_3 having a higher binding energy (~159.1 eV) than the fitted peak (158.6 eV).[52] A third doublet with a 1.2 eV splitting is attributed to sulfide S 2*p* peaks.[53] Due to overlap in the Bi 4*f* and S 2*p* spectra, additional peak fitting was conducted on the S 2*s* region to further analyze the sulfur species on the Cu_3BiS_3 surface. A singlet observed at 225.8 eV agrees with Cu_3BiS_3 films deposited by thermal evaporation and surface cleaned by Ar^+ ion sputtering, as no other studies have rigorously fit the peaks of the S 2*s* region.[11] A second singlet with lower intensity at higher binding energies was also fit and this may correspond to carbon contaminated sulfur species on the surface from air exposure.[11,54] The amount of surface contaminated sulfur and oxidic Bi species can be reduced through surface Ar^+ ion sputtering,[11] but our films show lower amounts of contaminated surface species compared to other reported Cu_3BiS_3 samples,[11,25,43,49] even when exposed to atmospheric conditions.

3.3 Thin film property measurements.

The band gap and absorption coefficient of the resulting Cu_3BiS_3 thin films were measured by UV-vis-NIR spectroscopy (**Figures S7,8**). An absorption coefficient $\alpha = 5.0 \times 10^4$ cm^{-1} (1.46 eV) was derived from the transmittance spectrum of the resulting 490-nm thick Cu_3BiS_3 thin film annealed to 400 ˚C, which increases to $\alpha = 1.1 \times 10^5$ cm^{-1} (2.2 eV). The band gap of our solution deposited thin film samples was measured using the inverse logarithmic (ILD) method, which was first proposed by Jarosińksi et al. and is derived from the Tauc method.[55] By using absorbance data as inputs, the ILD method provides accurate determinations of semiconductor band gaps and has been shown to have several advantages over the more commonly used Tauc or McLean methods (see Supporting Information). We applied the ILD method to absorption data derived from transmittance spectrum of a 490 nm Cu_3BiS_3 thin film (**Figure S9**). The experimental band gap of the Cu_3BiS_3 thin films was determined to be 1.47 eV. This optical band gap lies well within the previously reported experimentally reported band gaps for Cu_3BiS_3 (1.10–1.80 eV).[30]

The reciprocal of the line of best fit from the linear regression of the ILD plot gives the exponential factor (*m*), which informs the type of electronic transition. Wittichenite Cu_3BiS_3 has been calculated and experimentally confirmed to be a direct band gap semiconductor.[30] From this, one would expect an exponential factor *m* of 0.5 (slope of 2) for a direct band gap semiconductor. Importantly, Jarosińksi et al. shows that for direct band gap

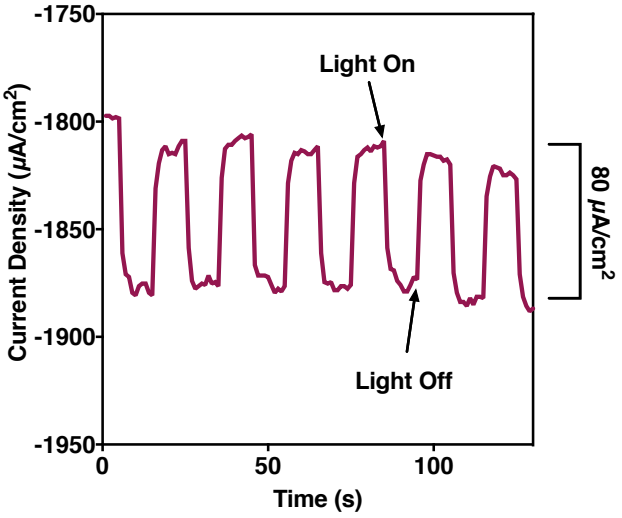

Figure 4. Transient photocurrent response of solution-processed Cu_3BiS_3 thin film deposited on FTO substrates in N_2-saturated 0.1 M $Eu(NO_3)_3$ (aq) under a potential of -800 mV *vs* Ag|AgCl (3 M KCl).

thin film samples of TiO_2 and MoS_2, the exponential factor yielded values of 1 because of the polycrystalline nature of the sputtered films, which affects the effective dimension and dispersion relations of the thin films.[55] We

find a similar *m* value of 0.98. From our experimental band gap and *m* value, we conclude our Cu_3BiS_3 thin films can be described as a direct band gap semiconductor.

Electrical conductivity of the Cu_3BiS_3 thin films was measured using the Van der Pauw geometry over the temperature range of 170-300 K. Temperature-dependent resistivity measurements suggest the resulting thin films behave like intrinsic semiconductors, where resistivity decreases with heating (**Figure S10**). A positive Hall coefficient with a carrier concentration of 4.2×10^{17} cm^{-3} was found at 300 K, indicating the *p*-type nature of our Cu_3BiS_3 thin films. The carrier concentrations decreased to 2.2×10^{13} cm^{-3} upon cooling to 170 K while carrier mobilities ranged from 0.4-90 cm^2 $(V\bullet s)^{-1}$ across the same temperature range. These values are consistent with those previously reported for thermally evaporated Cu_3BiS_3 thin films, with a carrier concentration of 2×10^{16} cm^{-3} and carrier mobility of 4 cm^2 $(V\bullet s)^{-1}$.[20]

The potential of using Cu_3BiS_3 as an effective solar absorber was further studied using transient photocurrent response measurements. The Cu_3BiS_3 thin films were interrogated in aqueous 0.1 M $Eu(NO_3)_3$, where the Eu^{3+} ions serve as the sacrificial oxidant. A calibrated AM1.5G filtered 300 W xenon arc lamp was used to measure the photocurrent response of the Cu_3BiS_3 with a graphite rod counter electrode and a Ag|AgCl reference electrode. Linear sweep voltammetry under chopped illumination shows cathodic photocurrent, which increases at potentials negative of -400 mV *vs* Ag|AgCl (**Figure S11**), further supporting the assignment of these Cu_3BiS_3 thin films as *p*-type semiconductors. The transient photocurrent response of a Cu_3BiS_3 thin film under chopped illumination at a fixed potential of -800 mV *vs* Ag|AgCl is given in **Figure 4**. This controlled potential electrolysis gave photocurrent densities >80 μA cm^{-2}; this current density exceeds those measured for *p*-type Cu_3BiS_3 thin films prepared by electrodeposition, which gave photocurrent densities of ~10 μA cm^{-2} at -350 mV *vs* Ag|AgCl under AM1.5G illumination.[25] To prove the photocurrent response resulted from Eu^{3+} reduction and not photocorrosion, we tested the photocurrent response over a 20 min period and found the response to be steady at 60 μA cm^{-2} (**Figure S12**).

4. CONCLUSIONS

We showed the utility of thiol-amine solvent mixtures to solution process phase pure Cu_3BiS_3 thin films using a semiconductor ink prepared by dissolving bulk CuO and Bi_2S_3 powders in the proper stoichiometric ratio. The resulting thin films possess a direct band gap E_g = 1.47 eV with a high absorption coefficient through the visible spectrum of $\alpha = 10^5$ cm^{-1}. We investigated the properties of the Cu_3BiS_3 thin films and confirmed that the electronic properties and photocurrent responses rival prior thin films of Cu_3BiS_3 prepared by other deposition methods.

The alkahest method has shown to be a reliable solution-based route for other high efficiency multinary chalcogenide thin film solar cells. We believe solution-processed Cu_3BiS_3 absorber layers, with its stable photocurrent response, highlight the potential for this material in solar energy conversion applications, including as potential photocatalysts or photodetectors.

CONFLICTS OF INTEREST

There are no conflicts to declare.

ACKNOWLEDGMENTS

R.L.B. thanks the National Science Foundation for support under DMR-1904719. We thank B. Melot, B. Tappan, L. Jordao, J. Intrator and M. Brady for assistance with data collection and analysis.

SUPPORTING INFORMATION

The Supporting Informatio is available free of charge on the ACS Publications website.

Additional experimental details, band gap determination from ILD method calculations, cross-sectional SEM micrographs, Rietveld refinement parameters, Raman spectrum, XPS spectra, transmittance and absorption spectra, ILD fitting plot, resistivity vs. temperature plot, photoelectrochemical linear sweep voltammogram and stability test (PDF)

REFERENCES

(1) Polman, A.; Knight, M.; Garnett, E. C.; Ehrler, B.; Sinke, W. C. Photovoltaic Materials: Present Efficiencies and Future Challenges. *Science* **2016**, *352*, aad4424.

(2) Fthenakis, V. M.; Morris, S. C.; Moskowitz, P. D.; Morgan, D. L. Toxicity of Cadmium Telluride, Copper Indium Diselenide, and Copper Gallium Diselenide. *Prog. Photovoltaics* **2000**, *7*, 489–497.

(3) Razykov, T. M.; Ferekides, C. S.; Morel, D.; Stefanakos, E.; Ullal, H. S.; Upadhyaya, H. M. Solar Photovoltaic Electricity: Current Status and Future Prospects. *Sol. Energy* **2011**, *85*, 1580–1608.

(4) Ganose, A. M.; Savory, C. N.; Scanlon, D. O. Beyond Methylammonium Lead Iodide: Prospects for the Emergent field of ns^2 Containing Solar Absorbers. *Chem. Commun.* **2017**, *53*, 20−44.

(5) Du, M. H. Efficient Carrier Transport in Halide Perovskites: Theoretical Perspectives. *J. Mater. Chem. A* **2014**, *2*, 9091–9098.

(6) Sun, J.; Singh, D. J. Electronic Properties, Screening, and Efficient Carrier Transport in $NaSbS_2$. *Phys. Rev. Appl.* **2017**, *7*, 024015.

(7) Sinsermsuksakul, P.; Sun, L.; Lee, S. W.; Park, H. H.; Kim, S. B.; Yang, C.; Gordon, R. G. Overcoming Efficiency Limitations of SnS-based Solar Cells. *Adv. Energy Mater.* **2014**, *4*, 1400496.

(8) Banu, S.; Ahn, S. J.; Ahn, S. K.; Yoon, K.; Cho, A. Fabrication and Characterization of Cost-Efficient $CuSbS_2$ Thin Film Solar Cells Using Hybrid Inks. *Sol. Energy Mater. Sol. Cells* **2016**, *151*, 14–23.

(9) Choi, Y. C.; Lee, D. U.; Noh, J. H.; Kim, E. K.; Seok, S. I. Highly Improved Sb_2S_3 Sensitized-Inorganic Organic Heterojunction Solar Cells and Quantification of Traps by Deep-Level

Transient Spectroscopy. *Adv. Funct. Mater*. **2014**, *24*, 3587−3592.

(10) Sugaki, A.; Shima, H. Phase Relations of the Cu_2S-Bi_2S_3 System. *Technol. Rep. Yamaguchi Uni.* **1972**, *1*, 71–85.

(11) Whittles, T. J.; Veal, T. D.; Savory, C. N.; Yates, P. J.; Murgatroyd, P. A. E.; Gibbon, J. T.; Birkett, M.; Potter, R. J.; Major, J. D.; Durose, K.; Scanlon, D. O.; Dhanak, V. R. Band Alignments, Band Gap, Core Levels, and Valence Band States in Cu_3BiS_3 for Photovoltaics. *ACS Appl. Mater. Interfaces* **2019**, *11*, 27033–27047.

(12) Kocman, V.; Nuffield, E. W. The Crystal Structure of Wittichenite, Cu_3BiS_3. *Acta Cryst.* **1973**, *29*, 2528−2535.

(13) Kumar, M.; Persson, C. Cu_3BiS_3 as a Potential Photovoltaic Absorber with High Optical Efficiency. *Appl. Phys. Lett*. **2013**, *102*, 062109.

(14) Mohan, R. Green Bismuth. *Nat. Chem*. **2010**, *2*, 336.

(15) *Mineral Commodity Summaries 2016*; U.S. Geological Survey, U.S. Government Printing Office: Washington, DC, **2016**, 36–81.

(16) Lokanc, M.; Eggert, R.; Redlinger, M. *The Availability of Indium: The Present, Medium Term, and Long Term*. National Renewable Energy Laboratory Report; U.S. Department of Energy: Golden, CO, 2015.

(17) Cao, J.; Choi, C. H.; Zhao, F. Agent-Based Modeling for By-Product Metal Supply–A Case Study on Indium. *Sustainability* **2021**, 13, 7881.

(18) Gerein, N. J.; Haber, J. A. Synthesis of Cu_3BiS_3 Thin Films by Heating Metal and Metal Sulfide Precursor Films under Hydrogen Sulfide. *Chem. Mater.* **2006**, *18*, 6289−6296.

(19) Gerein, N. J.; Haber, J. A. One-Step Synthesis and Optical and Electrical Properties of Thin Film Cu_3BiS_3 for Use as a Solar Absorber in Photovoltaic Devices. *Chem. Mater.* **2006**, *18*, 6297–6302.

(20) Mesa, F.; Gordillo, G.; Dittrich, T.; Ellmer, K.; Baier, R.; Sadewasser, S. Transient Surface Photovoltage of *p*-Type Cu_3BiS_3. *Appl. Phys. Let.* **2010**, *96*, 082113.

(21) Mitzi, D. B. Solution-Processed Inorganic Semiconductors. *J. Mater. Chem.* **2004**, *14*, 2355–2365.

(22) Liu, S.; Wang, X.; Nie, L.; Chen, L.; Yuan, R. Spray Pyrolysis Deposition of Cu_3BiS_3 Thin Films. *Thin Solid Films* **2015**, *585*, 72–75.

(23) Pai, N.; Lu, J.; Senevirathna, D. C.; Chesman, A. S. R.; Gengenbach, T.; Chatti, M.; Bach, U.; Andrews, P. C.; Spiccia, L.; Cheng, Y.-B.; Simonov, A. N. Spray Deposition of $AgBiS_2$ and Cu_3BiS_3 Thin Films for Photovoltaic Applications. *J. Mater. Chem. C* **2018**, *6*, 2483–2494.

(24) Colombara, D.; Peter, L. M.; Hutchings, K.; Rodgers, K. D.; Schafer, S.; Dufton, J. T. R.; Islam, M. S. Formation of Cu_3BiS_3 Thin Films via Sulfurization of Bi-Cu Metal Precursors. *Thin Solid Films* **2012**, *520*, 5165–5171.

(25) Kamimura, S.; Beppu, N.; Sasaki, Y.; Tsubota, T.; Ohno, T. Platinum and Indium Sulfide-Modified Cu_3BiS_3 Photocathode for Photoelectrochemical Hydrogen Evolution. *J. Mater. Chem. A* **2017**, *5*, 10450−10456.

(26) Deshmukh, S. G.; Patel, S. J.; Patel, K. K.; Panchal, A. K.; Kheraj, V. Effect of Annealing Temperature on Flowerlike Cu_3BiS_3 Thin Films Grown by Chemical Bath Deposition. *J. Electron. Mater.* **2017**, *46*, 5582–5588.

(27) Deshmukh, S. G.; Panchal, A. K.; Kheraj, V. Development of Cu_3BiS_3 Thin Films by Chemical Bath Deposition Route. *J. Mater. Sci.*, *Mater. Electron.* **2017**, *28*, 11926–11933.

(28) Deshmukh, S. G.; Kheraj, V.; Karande, K. J.; Panchal, A. K.; Deshmukh, R. S. Hierarchical Flower-Like Cu_3BiS_3 Thin Film Synthesis with Non-Vacuum Chemical Bath Deposition Technique. *Mater. Res. Express* **2019**, *6*, 084013.

(29) Li, J.; Han, X.; Zhao, Y.; Li, J.; Wang, M.; Dong, C. One-Step Synthesis of Cu_3BiS_3 Thin Films by a Dimethyl Sulfoxide (DMSO)-Based Solution Coating Process for Solar Cell Application. *Sol. Energy Mater. Sol. Cells* **2018**, *174*, 593−598.

(30) Deshmukh, S. G.; Kheraj, V. A Comprehensive Review on Synthesis and Characterizations of Cu_3BiS_3 Thin Films for Solar Photovoltaics. *Nanotechnol. Environ. Eng*. **2017**, *2*, 1–12.

(31) Webber, D. H.; Brutchey, R. L. Alkahest for V_2VI_3 Chalcogenides: Dissolution of Nine Bulk Semiconductors in a Diamine-Dithiol Solvent Mixture. *J. Am. Chem. Soc.* **2013**, *135*, 15722−15725.

(32) Antunez, P. D.; Torelli, D. A.; Yang, F.; Rabuffetti, F. A.; Lewis, N. S.; Brutchey, R. L. Low Temperature Solution-Phase Deposition of SnS Thin Films. *Chem. Mater.* **2014**, *26*, 5444−5446.

(33) McCarthy, C. L.; Webber, D. H.; Schueller, E. C.; Brutchey, R. L. Solution-Phase Conversion of Bulk Metal Oxides to Metal Chalcogenides Using a Simple Thiol-Amine Solvent Mixture. *Angew. Chem., Int. Ed.* **2015**, *54*, 8378−8381.

(34) McCarthy, C. L.; Cottingham, P.; Abuyen, K.; Schueller, E. C.; Culver, S. P.; Brutchey, R. L. Earth Abundant $CuSbS_2$ Thin Films Solution Processed from Thiol-Amine Mixtures. *J. Mater. Chem. C* **2016**, *4*, 6230−6233.

(35) McCarthy, C. L.; Brutchey, R. L. Solution Deposited $Cu_2BaSnS_{4-x}Se_x$ from a Thiol-Amine Solvent Mixture. *Chem. Mater.* **2018**, *30*, 304−308.

(36) McCarthy, C. L.; Brutchey, R. L. Solution Processing of Chalcogenide Materials Using Thiol-Amine "Alkahest" Solvent Systems. *Chem. Commun.* **2017**, *53*, 4888−4902.

(37) Koskela, K. M.; Melot, B. C.; Brutchey, R. L. Solution Deposition of a Bournonite $CuPbSbS_3$ Semiconductor Thin Film from the Dissolution of Bulk Materials with a Thiol-Amine Solvent Mixture. *J. Am. Chem. Soc.* **2020**, *142*, 6173–6179.

(38) Zhao, X.; Lu, M.; Koeper, M. J.; Agrawal, R. Solution-Processed Sulfur Depleted $Cu(In,Ga)Se_2$ Solar Cells Synthesized from a Monoamine-Dithiol Solvent Mixture. *J. Mater. Chem. A* **2016**, *4*, 7390-7397.

(39) Arnou, P.; van Hest, M. F. A. M.; Cooper, C. S.; Malkov, A. V.; Walls, J. M.; Bowers, J. W. Hydrazine-Free Solution-Deposited $CuIn(S,Se)_2$ Solar Cells by Spray Deposition of Metal Chalcogenides. *ACS Appl. Mater. Interfaces* **2016**, *8*, 11893–11897.

(40) Uličná, S.; Arnou, P.; Abbas, A.; Togay, M.; Welch, L. M.; Bliss, M.; Malkov, V.; Walls, J. M.; Bowers, J. W. Deposition and Application of a Mo-N Back Contact Diffusion Barrier Yielding a 12.0% Efficiency Solution-Processed CIGS Solar Cell Using a Thiol-Amine Solvent System. *J. Mater. Chem. A* **2019**, *7*, 7042–7052.

(41) Yakushev, M. V.; Maiello, P.; Raadik, T.; Shaw, M. J.; Edwards, P. R.; Krustok, J.; Mudryi, A. V.; Forbes, I.; Martin, R. W. Electronic and Structural Characterisation of Cu_3BiS_3 Thin Films for the Absorber Layer of Sustainable Photovoltaics. *Thin Solid Films* **2014**, *562*, 195–199.

(42) Yan, C.; Gu, E.; Liu, F.; Lai, Y.; Li, J.; Liu, Y. Colloidal Synthesis and Characterization of Wittichenite Copper Bismuth Sulphide Nanocrystals. *Nanoscale* **2013**, *5*, 1789–1792.

(43) Zhong, J.; Xiang, W.; Cai, Q.; Liang, X. Synthesis, Characterization and Optical Properties of Flower-Like Cu_3BiS_3 Nanorods. *Mater. Lett.* **2012**, *70*, 63–66.

(44) Hurma, T.; Kose, S. XRD Raman Analysis and Optical Properties of CuS Nanostructured Film. *Optik* **2016**, *127*, 6000−6006.

(45) Shuai, X.; Shen, W.; Hou, Z.; Ke, S.; Xu, C.; Jiang, C.; A Versatile Chemical Conversion Synthesis of Cu_2S Nanotubes and the Photovoltaic Activities for Dye-Sensitized Solar Cell. *Nanoscale Res. Lett.* **2014**, *9*, 1–7.

(46) Kaltenhauser, V.; Rath, T.; Haas, W.; Torvisco, A.; Müller, S. K.; Friedel, B.; Kunert, B.; Saf, R.; Hofer, F.; Trimmel, G. Bismuth Sulphide-Polymer Nanocomposites from a Highly Soluble Bismuth Xanthate Precursor. *J. Mater. Chem. C* **2013**, *1*, 7825–7832.

(47) Wang, J. J.; Akgul, M. Z.; Bi, Y.; Christodoulou, S.; Konstantatos, G. Low-Temperature Colloidal Synthesis of $CuBiS_2$ Nanocrystals for Optoelectronic Devices. *J. Mater. Chem. A* **2017**, *5*, 24621−24625.

(48) Hernádez-Mota, J.; Espíndola-Rodríguez, M.; Sánchez, Y.; López, I.; Peña, Y.; Saucedo, E. Thin Film Photovoltaic Devices Prepared with Cu_3BiS_3 Ternary Compound. *Mater. Sci. Semicond. Process.* **2018**, *87*, 37–43.

(49) Murali, B.; Madhuri, M.; Krupanidhi, S. B. Near-Infrared Photoactive Cu_3BiS_3 Thin Films by Co-Evaporation. *J. Appl. Phys.* **2014**, *115*, 173109.

(50) Lebugle, A.; Axelsson, U.; Nyholm, R.; Mårtensson, N. Experimental *L* and *M* Core Level Binding Energies for the Metals ^{22}Ti to ^{30}Zn. *Phys. Scr.* **1981**, *23*, 825–827.

(51) Biesenger, M. C.; Lau, L. W. M.; Gerson, A. R.; Smart, R. S. C. Resolving Surface Chemical States in XPS Analysis of First Row Transition Metals, Oxides, and Hydroxides: Sc, Ti, V, Cu, Zn. *Appl. Surf. Sci.* **2010**, *257*, 887–898.

(52) Debies, T. P.; Rabalais, J. W. X-Ray Photoelectron Spectra and Electronic Structure of Bi_2X_3 (X = O, S, Se, Te) *Chem. Phys.* **1977**, *20*, 277–283.

(53) Ge, J.; Yan, Y. Synthesis and Characterization of Photoelectrochemical and Photovoltaic Cu_2BaSnS_4 Thin Films and Solar Cells. *J. Mater. Chem. C* **2017**, *5*, 6406−6419.

(54) Lindberg, B. J.; Hamrin, K.; Johansson, G.; Gelius, U.; Fahlman, A.; Nordling, C.; Siegbahn, K. Molecular Spectroscopy by Means of ESCA II. *Sulfur Compounds*. *Correlation of Electron Binding Energy with Structure. Phys. Scr.* **1970**, *1*, 286–298.

(55) Jarosiński, Ł.; Pawlak, J.; Al-Ani, S. K. J. Inverse Logarithmic Derivative Method for Determining the Energy Gap and the Type of Electron Transitions as an Alternative to the Tauc Method. *Opt. Mater.* **2019**, *88*, 667–673.